THESIS FOR THE DEGREE OF LICENTIATE OF ENGINEERING IN THERMO AND FLUID DYNAMICS

Experimental Investigation of Cavitation-Bubble-Induced Atomization

JIAYI ZHOU

Department of Mechanics and Maritime Sciences

CHALMERS UNIVERSITY OF TECHNOLOGY

Gothenburg, Sweden 2019

Experimental Investigation of Cavitation-Bubble-Induced Atomization
JIAYI ZHOU

Technical report no 2019:15

Department of Mechanics and Maritime Sciences
Chalmers University of Technology
SE-412 96 Gothenburg
Sweden
Telephone + 46 (0)31-772 1419

Chalmers Reproservice
Gothenburg, Sweden 2019

Experimental Investigation of Cavitation-Bubble-Induced Atomization

JIAYI ZHOU
Department of Mechanics and Maritime Sciences
Chalmers University of Technology

Abstract

Improving the efficiency and lowering the emissions of internal combustion engines (ICE) has been drawing increased attention because climate change caused by greenhouse gases and the need to reduce emissions harmful to human health, and stricter legislation on the emissions from liquid-fueled transportation is implemented. Design of the liquid fuel atomizer, which atomizes the fuel delivered into the combustion chamber by the fuel injection system, is important because a good atomization, which facilitates the evaporation of fuel and improves the fuel-air mixture, leads to higher efficiency and lower emissions of ICE. Cavitation which originates inside the atomizer nozzle has great influence on the liquid atomization. Aiming at providing validation data of cavitation bubble collapse induced spray break-up for Computational Fluid Dynamics (CFD) simulation, which is a powerful tool for understanding the mechanism of atomization and the design of fuel atomizers, a series of experiments were carried out to investigate the influence of individual cavitation bubbles generated by laser light.

As a first step, to obtain information on laser-induced cavitation bubbles, an experiment was set up to investigate bubble formation in a glass cell (cuvette) filled with water. A pulsed Nd:YAG laser was used for bubble generation and for imaging, a schlieren set-up with an intensified CCD camera was used. Bubble generation, collapse, rebound, etc. was imaged, as well as the shock waves associated with these events. The relationship between bubble size and laser pulse energy was investigated.

As the next step, bubbles were generated close to the free water surface in the cuvette. A dimensionless variable γ, which is the distance of the initial bubble centroid to the free surface divided by the maximum bubble radius, was implemented. The experimental cases covered a wide range of γ values (from 0.86 to 2.24). Time resolved shadowgrams of bubbles and free surface deformations were used to analyze the bubble and free surface dynamics in different cases. The results showed the typical surface deformations of a fast spike jet and a slower thick jet at low γ values (<1.0), merged spike and thick jets when the γ value was in certain higher range (~1.1-1.3), and just protrusions for even higher γ values.

Finally, the effect of laser-induced cavitation bubbles on jet break-up was studied in a continuous flow rig, where the water exited from a transparent nozzle at various flow velocities. Shadow images of the jet or spray were recorded by a high-speed video camera. The break-ups induced by the bubble collapse, were measured, compared and analyzed under different injection pressures and bubble generating positions. The break-ups were categorized into small and massive breakups. The distance of the laser focus to the center axis of the nozzle was found to be the main factor that determined the type of break-up.

Keywords: liquid atomization, cavitation bubble, shadowgraph.

List of publications

The work in this thesis is based on the following papers:

I. Jiayi Zhou, Mats Andersson, Experimental study on free surface deformation induced by cavitation bubble collapse at different depths, submitted to Physical Review Fluids.

II. Jiayi Zhou, Mats Andersson, Break-up induced by the collapse of laser-generated cavitation bubbles in a liquid jet, 14th International Conference on Liquid Atomization and Spray Systems (ICLASS 2018), Chicago, IL USA, paper 181.

Acknowledgements

First I would like to thank my supervisor Mats Andersson. Mats is an expert on the optical experiment of sprays. He gave me a lot of suggestions on the design of my experiment setups. Mats has large amount of practical experiences on optical setups. He can always find the disadvantages in my setups, gave me valuable suggestions on how to improve the system. He also taught me some experiment skills which are tiny but can bring a lot of convenience to the experiments. He is very careful on correcting my papers and reports. And he is a responsible supervisor who is always able to discuss with me and solve my problems on my research.

I would like to thank Professor Mark Linne and Professor Ingemar Denbratt who hired and gave me the opportunity to work in the Division of Combustion and Propulsion Systems. Thank Professor Michael Oevermann who is my examiner with guidance on my project.

As an experimentalist working in cell G, I cannot run my experiments without the help from our research engineers. I would like to thank Patrik Wåhlin, Alf Magnusson who gave me a lot of supports on my experiments. Patrik is a very reliable engineer who is always happy to help me and answer my questions no matter on the experiments or on the work of my home. His suggestions are always professional and helpful. Thank Alf for giving me the nitrogen bottle and the carefully security check and mount of it.

Thanks for the financial support from the Holistic Approach of Spray Injection through a Generalized Multi-phase Framework (HAoS) project which is a Marie-Skłodowska-Curie Innovative Training Network of the European Union's Horizon 2020. Thanks for giving me the opportunity to collaborate with other participants in the network.

Many thanks to our financial officer Elenor Norberg who is always kind and willing to help me. Thank my office mates Sreelekha Etikyala and Kristoffer Clasén. I had a lot of happy time with them both in and outside the office. Thank Doctor Chengjun Du who helped me a lot when I just came to Sweden and Doctor Zachary Falgout who helped me to get familiar with the experiment setups.

Last but not the least I would like to thank my parents who are always supporting and trusting me. Without their support, I wouldn't be able to get my master degree in China and continue my academic career in Sweden.

Contents

1 Introduction

Cavitation is a quite common phenomenon which can be found in many occasions such as flow inside tubes, fluid surrounding a rotating propeller, fluid in an ultrasonic field, and so on. Cavitation happens when a liquid is subjected to a decreasing pressure which falls below the saturated vapor pressure [1]. The collapse of the vapor cavities, often called cavitation bubbles, has drawn a lot of research attention especially for the collapse close to the liquid-gas or liquid-solid interface [2-8]. The expansion, collapses, and rebounds of the cavitation bubble close to the liquid-gas interface usually result in deformation of the free surface and aspherical shape of the bubble. Visualizations of bubble growth and free surface deformation are usually done by high speed imaging experiments. In these experiments, cavitation bubbles are introduced in the vicinity of the free surface by generating a breakdown in the liquid with electrodes or a focused laser beam [9-14]. Unlike the spherical expansion, collapse and rebound of a cavitation bubble which is introduced in an infinite liquid, the expanding cavitation bubble near a free surface is becoming prolate. As the bubble is collapsing, a spike jet comes out of the surface and a counter micro-jet growing apart from the surface forms inside the bubble. The counter jet makes the shrinking bubble deformed on the side, which is towards the surface, and breaks the bubble into two parts. As the bubbles are rebounding, a thicker jet comes out of the surface. The free surface deformation and aspherical collapse of bubble described above are typical interaction of a collapsing bubble and free surface.

Deformations of the liquid-gas interface have also been investigated with various applications in mind, such as underwater explosion [15-21], the laser-induced forward transfer technique (LIFT) [12,13,22-26], jet primary break-up [27], needle-free injection systems (NFIS) [4] and so on. Nowadays more and more attentions are being paid to the research on lowering the emissions from internal combustion engines (ICE) because the climate change caused by greenhouse gases as well as other harmful emissions is becoming a severe problem and governments of various countries and organizations are implementing stricter legislations on the emissions from liquid-fueled transportation. The fuel injection system, which delivers liquid fuel into the combustion chamber and makes it evaporate and mix with air, can contribute for an efficient combustion with low emissions with a properly designed fuel atomizer. Cavitation which originates close to the sharp edge at the inlet of the nozzle of a liquid atomizer [28] is believed to be an important mechanism causing atomization in the sprays [29]. To investigate the cavitation inside the nozzle and its effect on fuel atomization, numerous optical diagnostic methods have been applied to observe and detect the flow inside and outside the nozzle. Usually, internal flow is visualized by using transparent nozzles and shadowgraph imaging with high speed cameras. The cavitation region which contains cavities and bubbles appears darker than the liquid phase ambient in the shadowgraph images, because the refraction index of the gas phase is different from that of liquid phase. Particle image velocimetry (PIV) is applied to measure the velocity of in-nozzle flow [30,31]. Since it is difficult to measure liquid velocity, turbulence intensity and radial distribution cavitation inside a cylindrical nozzle, studies have been carried out by using two-dimensional (2D) transparent nozzles for visualizing detailed cavitation behavior [32]. The velocity and droplet size distribution of spray outside the nozzle can be measured by Phase Doppler Anemometry (PDA) [33]. Shadowgraph imaging gives the whole view and outskirt behavior of spray, but it is hard to look into the inside of the optically

dense region of a spray. Thus, other imaging methods have been developed to solve this problem, for example, Ballistic imaging (BI), X-ray imaging, and structured laser illumination planar imaging (SLIPI) [34]. Compared to the ones inside the nozzle, cavitation bubbles outside the nozzle are more difficult to observe because they are surrounded by droplets and liquid phase jet. To solve this problem, a special near-nozzle field visualization of cavitation bubbles has been carried out by injecting the fuel in a liquid environment of a pressurized fuel chamber [35].

For the design of fuel injection systems, beside the experimental investigations, simulation tools are quite important for understanding the complex multiphase flow processes during fuel injection as well. Direct Numerical Simulation (DNS) is an ideal tool because of its possibility to achieve 'all scale' analysis. However, it is restricted by the current computational capabilities, and not applicable at the high Reynolds numbers encountered in the fuel injection systems. Large Eddy Simulation (LES) is a computationally more affordable alternative, but closure models are needed for resolving the unresolved sub-grid-scale (SGS). Therefore, the Holistic Approach of Spray Injection through a Generalized Multi-phase Framework (HAoS) project [36], which is targeting the development of a LES CFD model that accounts for the influence of unresolved SGS processes to engineering scales at affordable computing time scales, was established. Relevant SGS closure models are developed supported by data from tailored experiments and DNS and will be implemented into the LES model.

Current SGS models lack some key fluid dynamics such as in-nozzle cavitation, bubble collapse, shock wave effects and so on. Therefore, investigation of the influence of a single bubble collapse on jet break-up is necessary. Although a lot of experimental studies have been done on both bubble collapse induced free surface deformation and the effect of cavitation on spray atomization as mentioned before, there are relatively few studies on single cavitation bubble collapse-induced jet or spray break-up. Therefore, the current project, which is the study of bubble collapse-induced spray break-up, was embedded into the experimental work package of the HAoS project.

So far the studies of single bubble collapse in liquid jets are limited in laminar flow jet and square-shaped jet. Robert et. al. [37] studied the growth and collapse of laser-induced cavitation bubbles inside free-falling liquid water jets. The maximum speeds of ejected microjets and droplets were recorded and found to be affected by the jet diameter ratio and eccentricity coefficient. The growth and collapse of a bubble between two parallel free surfaces were investigated experimentally and numerically by Ogasawara et. al. [38]. The parallel free surfaces were generated by a nozzle which has a rectangular cross-section outlet. Shadow images of the bubbles inside the jet and deformations of the free surfaces were recorded by high speed video camera.

The progress of the current thesis work, where the dynamics and effects of individual cavitation bubbles was investigated in various geometries can be summarized as following:

As a first step, to offer the information of laser-induced cavitation bubbles, an experiment was set up to investigate bubble formation in a glass cell (cuvette). A pulsed Nd:YAG laser was

used for bubble generation and for imaging, a schlieren set-up with an intensified CCD camera was used. Bubble generation, collapse, rebound, etc. was imaged, as well as the shock waves associated with these events. The relationship between bubble size and laser pulse energy was investigated.

As the next step, bubbles were generated close to the free water surface, and besides the bubble and shock wave dynamics, different kind of ejection events were identified, such as narrow spikes, broader structures, and separating drops. The evolution of the bubbles and structures with time, for different bubble depths was studied. This work was presented in Paper I.

Finally the effect of laser-induced cavitation bubbles on jet break-up was studied in a continuous flow rig, where the water exited from a transparent nozzle at various flow velocities. Cavitation bubbles were artificially introduced in the jet by focusing the laser light at several positions in the jet relative to the central jet axis. The flow outside the nozzle was imaged with a high-speed video camera. Due to the turbulent flow conditions the detailed characteristic of the individual break-up events varied and a statistical analysis — projected spray area change rate was applied. This work was presented in Paper II.

2 Experiment setups

2.1 The experiments with a cuvette

Figure 1 shows the experiment setup with the cuvette. The optical setup consisted of two main parts which were the laser focusing arm and the Schlieren or shadowgraph imaging arm. The laser focusing arm was composed by a laser, an attenuator, a concave lens (L4) and two convex lenses (L5, L6). The laser was a neodymium-doped yttrium aluminium garnet (Nd:YAG) one which could provide 6-nanosecond laser pulses with the wavelengths of 1064, 532, 355, and 266 nm under Q-switched mode. The attenuator was composed by a half wave plate and a Glan-laser prism. They were put between the mirror and L4 and used for attenuating and adjusting the laser power. L4 was a concave lens whose focal length was -20 mm, and L5 was a convex lens with a focal length of 100 mm. L4 and L5 composed a beam expander of 5 times expansion. The laser beam was first expended by the beam expander and then focused into the cuvette by L6. The aim of expanding the laser beam before focusing it into the cuvette was providing a larger focusing angle to generate a compact plasma and, hence, a spherical bubble [6]. All these lenses were visible light antireflection coated and achromatic doublets to make sure only one single plasma formed at the focal point. The Schlieren or shadowgraph arm consisted of a lamp, a microscope (L1), a pinhole, two convex lenses (L2, L3), a sharp edge and a camera. L1 was a microscope with magnification of 20 times and numerical aperture (NA) of 0.4. The purpose of using a microscope was focusing the divergent light source in a short focal length which was hard to realize with a regular lens. The diameter of the pinhole was 300 μm. The lamp, microscope and pinhole composed an approximate point light source which provided sharper Schlieren images. The light beam which was collimated by L2 passed through the cuvette and was then focused at the sharp edge. The sharp edge was a normal razor blade. The sharp edge enabled visualization of density fluctuation of the medium between L2 and L3 along one dimension which was sufficient for observing the circular shockwaves. When performing the shadowgraph imaging, the sharp edge can be removed. The cuvette was made of optical glass. In the experiments, the cuvette was filled with deionized water. The aim of setting up a Schlieren system was to observe the shockwaves of optical breakdown and of the collapse of the bubble, and measuring the time interval between the two shockwaves. The laser and the camera were synchronized by a photodiode which detected the laser light reflected by a window and triggered the camera. Since the propagating velocity of the shockwave could be as fast as 1500 m/s, the camera should be fast enough to capture the shockwaves, otherwise, they may disappear from one frame to the next [39]. Thus, an intensified CCD (ICCD) camera (PI-Max 4) with short exposure time was put behind the sharp edge to take images of bubbles and shockwaves.

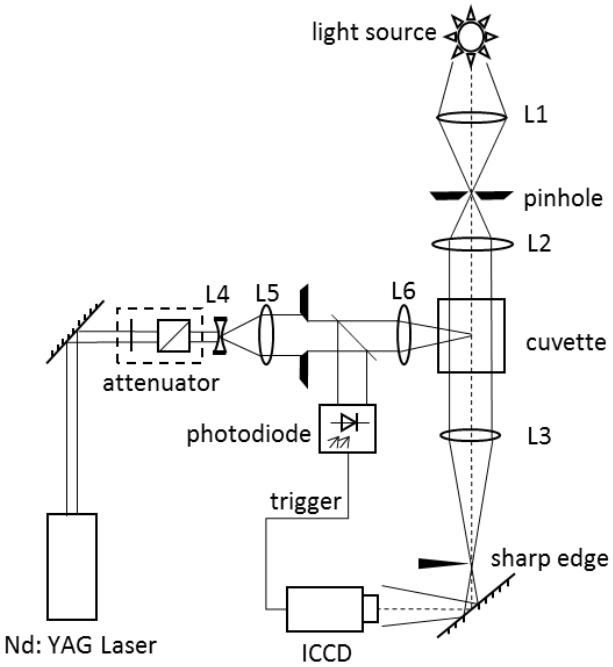

(a)

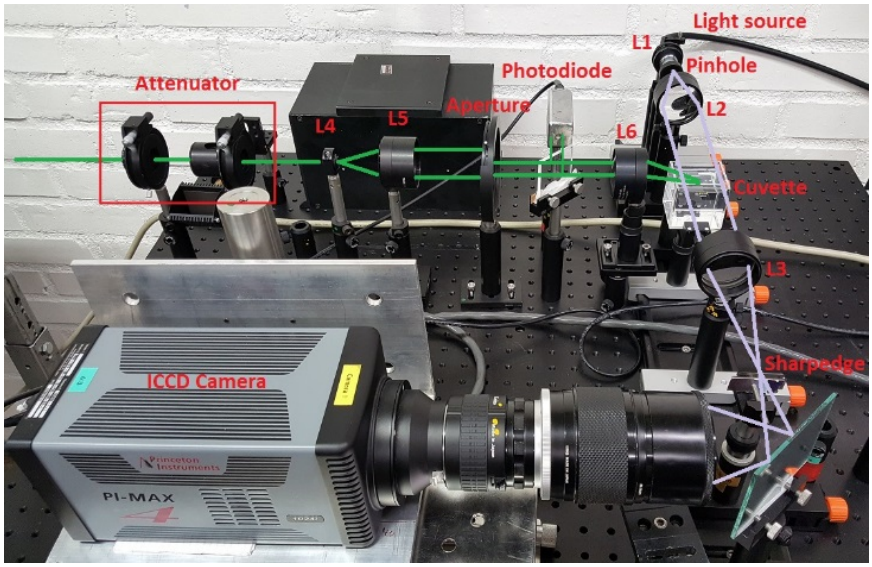

(b)

Figure 1 Schematic (a) and photo (b) of the experiment setup with the cuvette.

2.2 The experiment with a continuous flow rig

The effect of laser-induced cavitation bubbles on spray break-up was studied by using a continuous flow rig, where the liquid exited from a transparent nozzle. The continuous flow rig is shown in Figure 2. The nozzle was installed at the bottom of a volume which contained the liquid. The cylinder was held by two vertically mounted electric motor-driven translation stages. The relative vertical position of the laser beam focused to the nozzle orifice was varied by adjusting the height of the accumulator together with the nozzle via these two translation stages. The pipe P1 was connected to a nitrogen bottle which was the high-pressure source of

this rig, and controlled by the valve V1. The injection pressure was adjusted by a pressure regulator connected to the nitrogen bottle. Pipe P4 was the outlet of the cylinder. When the cylinder was filled up, the excess liquid flowed out through the naturally open valve V2 and P4. V1 and V2 were controlled by air pressure via P2. During injection, V1 was open and V2 was closed. The high-pressure nitrogen from P1 pressurized the liquid in the cylinder and pushed the liquid out through the nozzle at bottom. The injection pressure was measured by a force sensor inside the cylinder. The force sensor was connected to a computer by the green cable in Figure 2.

Figure 2 Photo of the continuous flow rig.

A schematic and a photo of experiment setup with continuous flow rig are shown in Figure 3. The experiment setup consisted of three main parts which were liquid injection, as described above, shadowgraph imaging, and laser beam focusing. The shadow imaging and laser focusing parts were similar to the cuvette setup. The shadowgraph part had a plasma lamp acting as the light source. The diverged light source was collimated by lens L1. The collimated light passed through the near nozzle orifice region to illuminate the primary break-up region of the spray. The high-speed video camera located at the other side of the nozzle captured shadowgraph videos of the spray. A filter was put in front of the camera lens to block scattered laser light. The laser beam focusing part contained a Nd: YAG laser which could provide ns-laser pulses. The power of the laser beam was reduced by the attenuator which was composed of a half wave plate and a Glan-laser prism. The energy was adjusted by rotating the half wave plate with a micrometer screw for fine tuning. The energy-reduced laser beam was expanded by the concave lens L2 and the convex lens L3, and then focused under the nozzle by focal lens L4. Lens L4, mounted on a micrometer translation stage, could be moved along the laser beam direction. In this way, the horizontal position of the beam focus could be varied by moving lens L4.

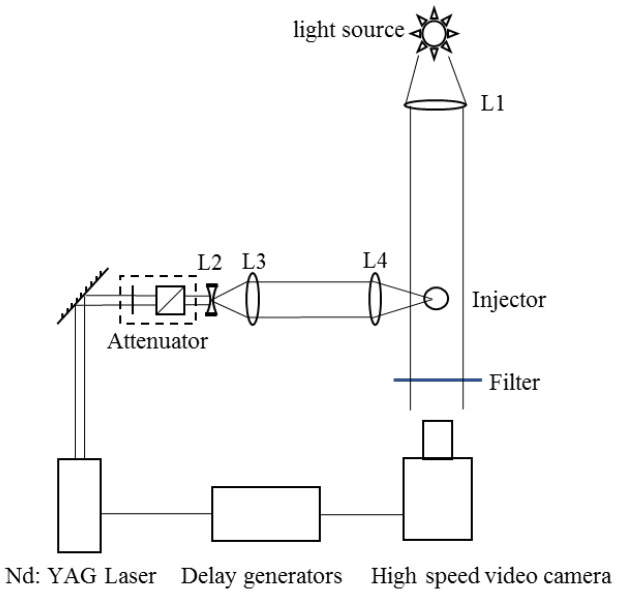

(a)

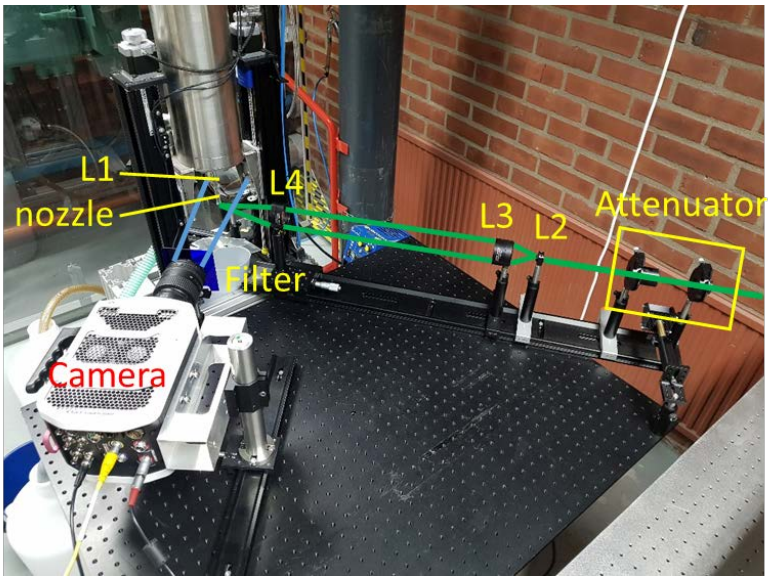

(b)

Figure 3 Schematic (a) and photo (b) of the experiment setup with the continuous flow rig.

In the experiment, the Nd: YAG laser and the high-speed video camera were synchronized by delay generators. The laser was triggered by a delay generator externally. The pulse energy, wavelength and frequency of the laser were 5 mJ, 532 nm and 10 Hz respectively. The frame synchronization signal of the camera was externally provided by the delay generators. The sample rate was 40000 fps. The camera was controlled to start to capture before each laser pulse with a time gap of 297 μs, and pause after 4.9 ms which was the length of each video fragment. The distance between the laser focus and the axis of nozzle varied from 1 mm to 3.5 mm with an interval of 0.5 mm. The liquid used in the experiment were deionized water and water-

dipropyleneglycol blends. The injection pressure was set to be from 1 bar to 6 bar over atmosphere with an interval around 0.5 bar. The ambient pressure was atmosphere. During each injection, there was a steady flow period of several seconds (depending on the pressure). The flow conditions for water in the form of Reynolds numbers with respect to injection pressures are shown in Table 1. The data are based on the mass flow rate measurements.

Table 1 The flow conditions for water in the form of Reynolds numbers with respect to injection pressures.

Injection pressure (bar)	1	1.5	2	2.5	3	3.5	4	4.5	5	5.5	6	6.5
Re ($\times 10^5$)	1.13	1.42	1.79	2.14	2.55	2.78	3.45	3.99	4.46	5.18	5.52	5.94

3 Free surface deformation induced by bubble collapse

3.1 Bubble introduction far from the free surface

As a first step, to learn how to control bubble formation and get the basic information about laser-induced cavitation bubbles, the bubbles were introduced into a cuvette filled with water. Images of typical laser-induced cavitation bubbles, recorded at different times after the laser pulse, are shown in Figure 4. The bubbles were introduced with 5 mJ laser pulses. At 0.9 µs after the laser pulse, a circular shockwave caused by the optical breakdown could be observed around the bubble. At 140 µs, the bubble reached its maximum diameter. At 235 µs, the bubble was collapsing and was about to rebound. At 300 µs, the bubble was rebounding after the first collapse.

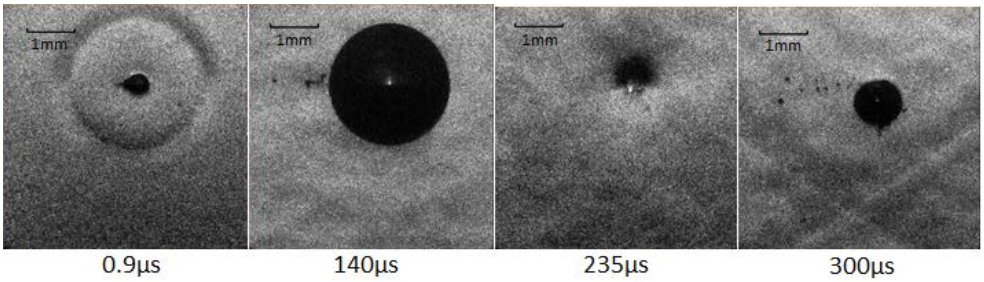

Figure 4 Cavitation bubbles introduced with 5 mJ pulses at different times after the laser pulse.

Bubbles were introduced in the cuvette with different laser pulse energies. To find out the relationship between pulse energy and the bubble size, a series of experiments were carried out and the results are shown in Figure 5. Figure 5 shows time-resolved averaged bubble diameters at different laser pulse energy. As the laser pulse energy increases, the maximum diameter of the bubble is larger, and the period of the bubble growth and collapse is longer. For the case of 7 mJ pulse energy, several cycles of bubble rebound and collapse after the first cycle are also shown in Figure 5. The maximum bubble diameter during each cycle becomes smaller and smaller due to the energy loss, and the period of the cycles becomes shorter and shorter as well. More detailed information on maximum bubble size and approximate duration before the first rebound are shown in Table 2. Table 2 also includes the maximum bubble diameter data from Vogel et. al. [39]. The bubble sizes in the current study are bigger probably due to the different liquid used in [39]. Deionized water was used in this study, while physiologic saline solution was used in Vogel's experiment.

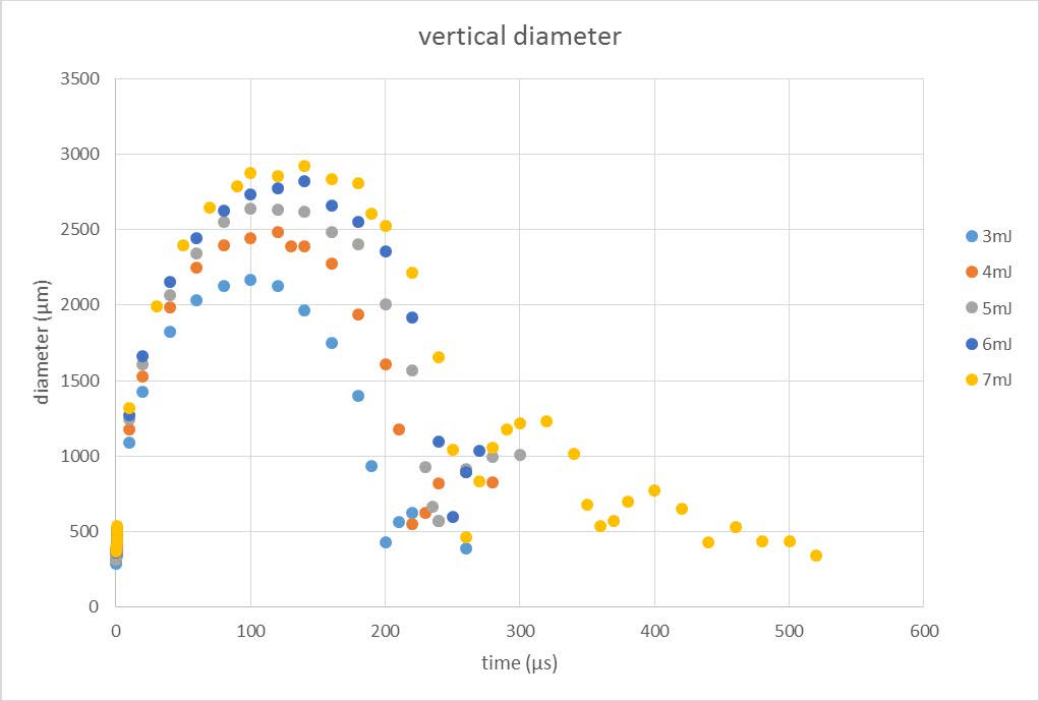

Figure 5 Time-resolved bubble diameters of different laser pulse energy.

Table 2 The average maximum bubble diameter and approximate duration before the first rebound.

Pulse energy (mJ)	3	4	5	6	7
Maximum diameter (mm)	2.17	2.48	2.64	2.82	2.92
Maximum diameter (mm) [39]	1.62	1.84	1.84		
Duration before the first rebound (μs)	200	220	240	250	260

3.2 Bubble introduction close to the free surface

The dynamics and mechanisms of bubble growth and collapse, and associated free surface jets have been studied profoundly with both experimental and simulation approaches. However, only few of the studies [12,40] payed attention to the second jet especially for the cases of relatively large bubble-surface distance when the first jet is comparatively weak or even does not form. In this study, both the spike and thick free surface jets were imaged together with the evolving cavitation bubble. The laser-induced cavitation bubbles were introduced into deionized water with different distances to the free surface. The experiments covered a relatively large range of bubble-surface distance to observe the cases with both the spike-like first free surface jets and second thick jets, and the cases with weak first jets, as well as the cases with only protrusions but no jet.

3.2.1 Relation between bubble size and distance to the surface

Bubble and free surface systems have been studied in many research fields and the size of the bubbles can vary from micrometer-range, e.g., the studies of LIFT [12,13,22-26], to meter-range, e.g., the studies of under-water explosion [15-21]. However, similarities can be found in these studies. When specifying the problem of bubble collapse near a free surface, a dimensionless variable γ, which is the distance of the initial bubble centroid to the free surface with respect to the maximum bubble radius, is frequently implemented. For example, Blake et al. [41] studied the growth and collapse of vapor bubbles generated at different γ values, where the bubbles were simulated and described by using boundary-integral approach. In the literature [12,13,42], the evolution of the vapor bubble volume and the evolution of spike jets and thick jets under different γ values have been recorded and compared. An illustration of this parameter is shown in Figure 6. In this figure, R_m is the maximum bubble radius, d is the distance of the initial bubble centroid to the free surface. It should be noted that the 'd' denoted in the sketch is not exactly the same as the initial bubble to surface distance d. When the bubble grows to its maximum size, the distance may change slightly. The γ value is defined as

$$\gamma = \frac{d}{R_m}$$

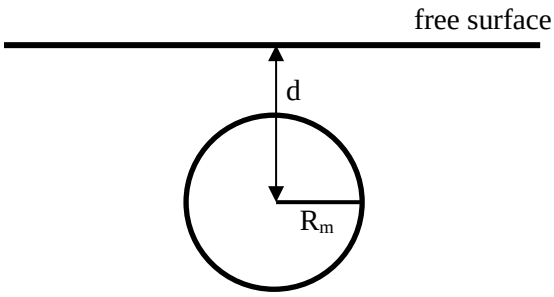

Figure 6 Sketch of the parameters of a cavitation bubble close to the free surface.

3.2.2 Experimental results

Different experimental cases were achieved by changing the position of the laser focus with respect to the surface, and thereby the γ value, which varied from 0.86 to 2.24. All the time-resolved images presented in Figure 7 were captured by an ICCD camera. Each image shows a shadowgram of the vicinity of the free surface after the laser-induced optical breakdown with a certain time delay. The time indicated below each image is the time interval between the moment when the camera received the signal from the photodiode which detected a laser pulse and the opening of the camera gate. Figure 7 (a), (b) and (c) represent experimental cases of γ = 0.86, 1.10 and 1.52 respectively. Figure 7 (a) shows a typical case of bubble collapse-induced free surface deformations when the dimensionless variable γ was 0.86. As the cavitation bubble was growing to its maximum diameter from the beginning to 0.1 ms, the free surface was deformed. During the collapsing phase of the bubble from 0.1 ms to 0.2 ms, a spike jet formed at the surface due to the high pressure spot between the upper surface of bubble and the free surface [41]. The spike jet continued growing, while a thicker jet formed at around 0.3 ms as the rebounded bubbles were growing and collapsing. The formation of the thick jet was due to

the expansion and collapse of the toroidal bubble (from 0.2 ms to 0.3 ms) which formed during the collapse of the original bubble (from 0.15 ms to 0.2 ms) [13].

Shadowgraphs of the case of a larger γ value of 1.10 are shown in Figure 7 (b). Similar to the case shown in Figure 7 (a), both spike and thick jets were found on the free surface. However, the spike jet grew much slower compared to the one seen in Figure 7 (a). Furthermore, it was even slower than the thick jet that came after it. The heights of the spike and thick jets became almost the same at 1.5ms. After 1.5ms, it was impossible to distinguish the spike jet from the thick jet because they merged together since the thick jet caught up with the spike jet. After the merge, the combined jet continued growing for several milliseconds.

Since the thick jet can grow faster and catch up with the spike jet at certain conditions, for example, when γ=1.10 and 1.27, it is possible that when the γ value becomes even larger, there will only be a thick jet or deformation without spike jet. Figure 7 (c) shows the shadow images of the free surface deformation when the γ value was 1.52. When the bubble was collapsing at 0.2 ms, the free surface was not yet disturbed, although the bubble itself was aspherical just like the ones in the cases mentioned before. After a relatively long time, deformation of the free surface was observed at 1 ms when the bubble had moved far away from the free surface, broken into tiny bubbles and almost dissolved in the water. The deformation was growing higher and narrower until 7 ms, after which it dropped down into a wider shape. The main difference of the free surface deformation in this case compared to the cases of lower γ values was that there was no jet or liquid detachment, only a wider protrusion formed at a longer time after the bubble generation.

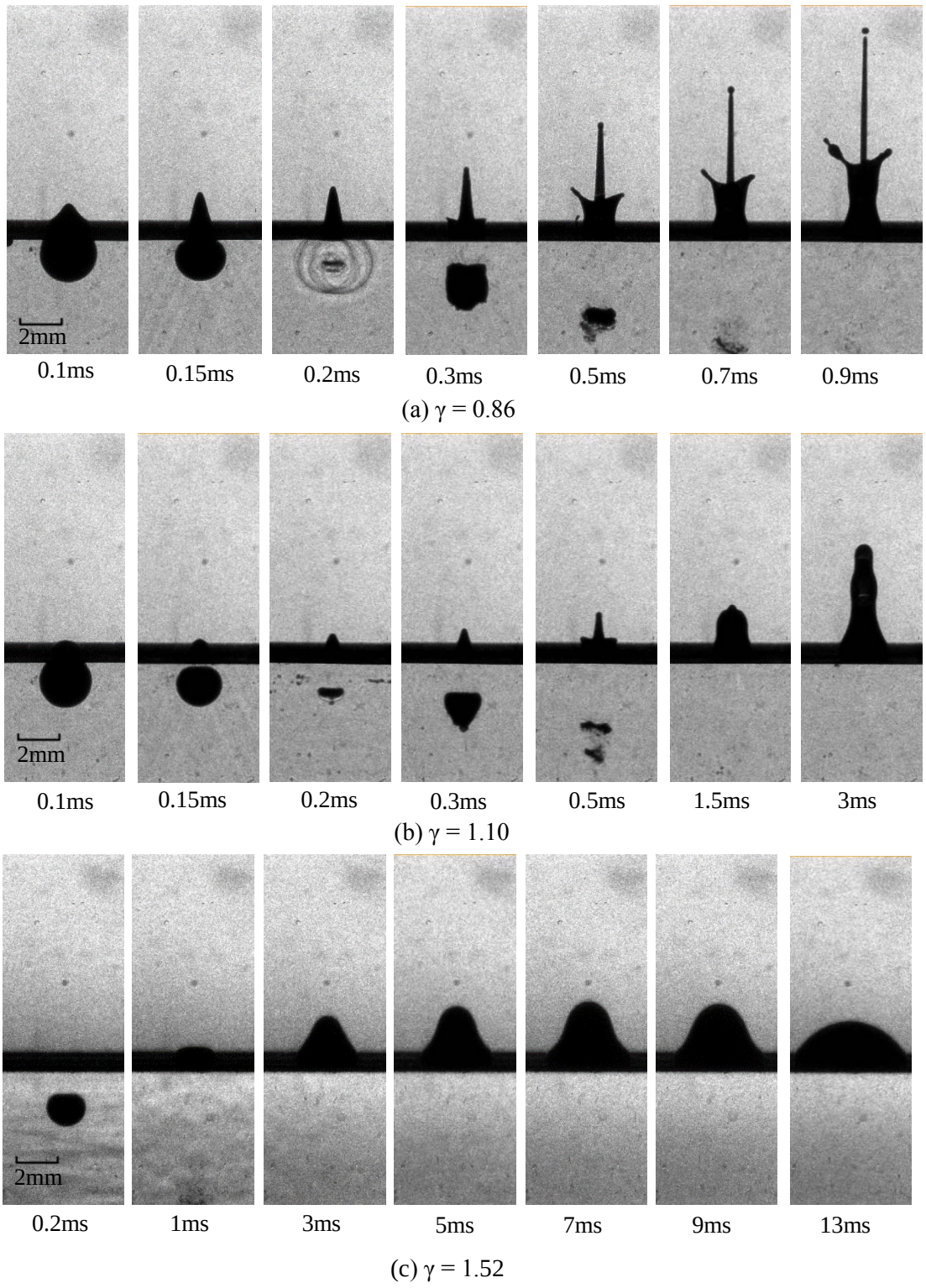

Figure 7 Images of cavitation bubble collapses and free surface deformations when (a) γ=0.86, (b) γ=1.10, (c) γ=1.52. Note the different time sequences.

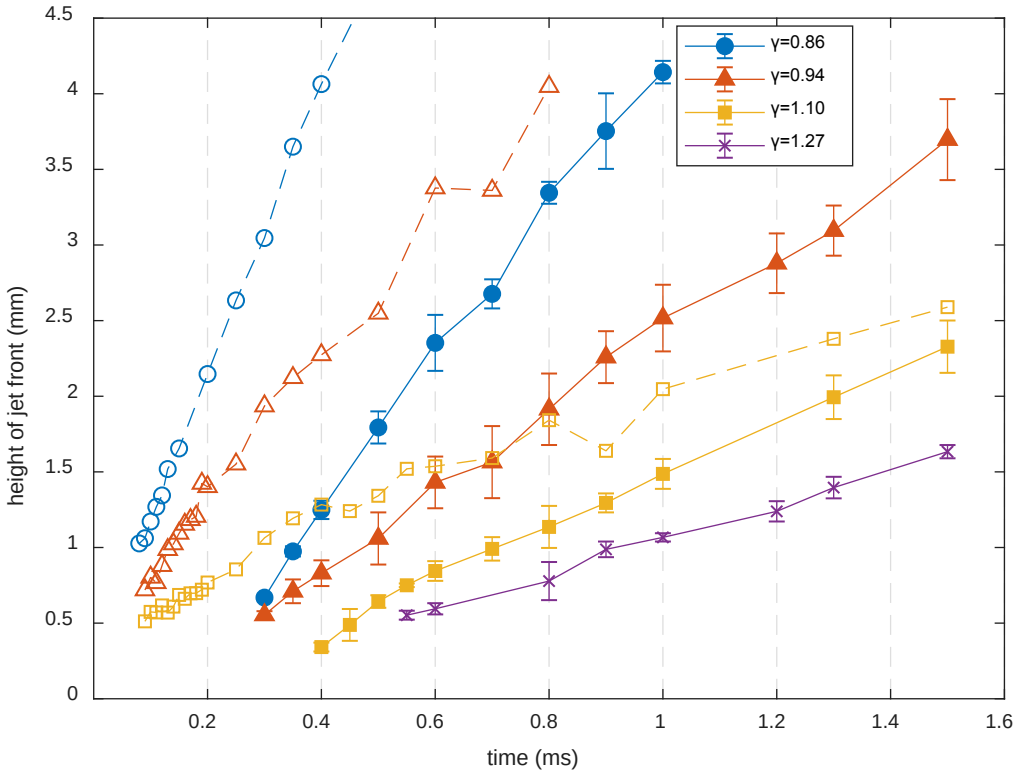

Figure 8 Heights of the spike (dash lines, open symbols) and thick (full lines, filled symbols) jet fronts when γ=0.86, 0.94, 1.10 and 1.27.

Figure 8 shows the height evolution of the spike and thick jet fronts of different γ values to give a clearer comparison. The dash and solid curves represent spike and thick jets respectively. When the γ value was getting larger, the growth of both spike and thick jets became slower. The case of γ=1.27 was similar to γ=1.10, but there was no clear spike jet, only a small deformation on the surface before the second jet emerged. Similar to the case of γ=1.10, the first deformation and thick jet merged together after 1.5 ms. By comparing the dash curves with the corresponding solid curves with the same color and same mark, it is clear that for the cases of γ=0.86 and 0.94, the thick jets were slower than the spike jets, while for the case of γ=1.10, the thick jet was faster than the spike jet and would catch up with the spike jet according to the trend of these two curves. For the cases of γ=0.86, 0.94 and 1.10, detached droplets were found on the top of the spike jets, while there was no such droplet found in the case of γ=1.27.

Similar structures of the free surface deformations include the spike jets and thick jets were also found in the studies by Patrascioiu et. al. [12] and Zhang et. al. [40] at the conditions of similar γ values. However, for the smaller scale bubble collapse [12], the thick jet front was rounder and without the crown shape, while for the larger scale bubble collapse [40], the thick jet front was more violent.

More details of the study can be found in Paper I.

4 Bubble collapse induced liquid jet break-up

Spray atomization can be enhanced by the collapse of cavitation bubbles [27,32,43,44]. However, studies specifically on the bubble collapse induced atomization without the influence of other mechanisms such as turbulence are quite rare. In this section, results of the liquid jet break-up induced by a single laser generated bubble collapse are presented and discussed.

The shapes of break-ups induced by collapse of cavitation bubbles varied a lot at different experimental conditions. Even for the same conditions, the break-ups could be different from pulse to pulse due to the turbulent character of the jet and its non-smooth surface. However, regularities were found after some qualitative and quantitative analysis. In this study the main parameters varied were the distance between the laser focus and the axis of the nozzle, and the injection pressure, denoted as ‘d’ and ‘P’ respectively. An illustration of the distance d is shown in Figure 9.

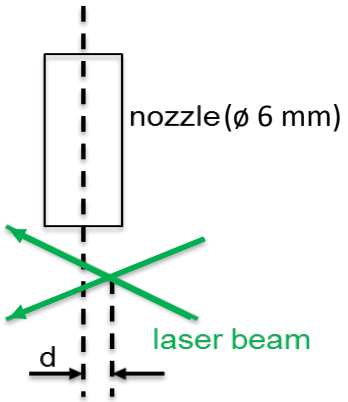

Figure 9 Sketch of the laser focus position with respect to the central axis of the nozzle hole.

Based on their shapes, the break-ups can be divided into two types. One is called small break-up shown in Figure 10 (a), the other is massive break-up shown in Figure 10 (b). The presented images are chosen from two different video sequences which were taken at different experimental conditions; for Figure 10 (a), d=1.5 mm, and P=1.6 bar, while for Figure 10 (b), d=2.5 mm, P=3.6 bar. The time under each frame is counted from the moment of the laser pulse emission. For the small break-up, there is only one main spike ejected from the jet. The tip of the spike separates into tiny droplets quickly, and is followed by a ligament which breaks up later as well. During the recording period, there are relatively few spontaneous break-ups besides the one induced by the collapse of the artificially introduced cavitation bubble. For the massive break-up shown in Figure 10 (b), multiple ejected spikes are breaking up from the jet at 0.1 ms. Then at 0.5 ms, a large fragment is coming out of the jet. The fragment is separating into more ligaments at 1 ms and 1.5 ms. At last, these ligaments are breaking into droplets as is shown in the image of 2 ms. During this recording period, due to the increased injection pressure resulting in a higher jet velocity, there are more spontaneous break-ups beside the one induced artificially. However, the cavitation bubble induced break-up comes earlier and spreads wider in the radial direction of jet.

To figure out which factor affects the break-up type most, a quantitative analysis of projected spray area change rate was performed. The images were first binarized to identify the area where liquid is present. The binarization keeps the main body of the jet and the large break-up structures like large droplets, the ejected spikes, and fragments shown in Figure 10, while it discards the droplets that are too small to be distinguished from the background noise or move too far away from the jet. The normalized projected spray area is the ratio of the number of the pixels that are 1 to the amount of all pixels in the selected region. In Figure 11, the change rate is the difference of the normalized spray area between consecutive images with respect to time. Figure 11 shows the results at the conditions of d=1 mm to d= 3.5 mm when the injection pressure is 1.1 bar. These are the averaged results from 15 repetitive experiments except the d=1 mm case which is the average of 2 samples, since most events with d=1 mm did not produce clearly identifiable break-ups. For most cases, there is an obvious peak right after 0 ms when the laser pulse arrives. The rapid increase of the area change rate represents the fast development of the bubble collapse induced break-up right after the laser pulse. The highest peak is found at d=2.5 mm. For most cases except d=2.5 mm, the area change rate decreases rapidly to around zero, which means the relatively large break-up structure only exists for a short time after the laser pulse and separates into tiny droplets quickly. The small break-up shown in Figure 10 (a) fits this result. For d=2.5 mm, there is an extended decreasing slope crossing the zero change rate level at around 2 to 2.5 ms. This extended slope shows that the large break-up structures continue developing for longer time before they turn into tiny droplets. The negative part of the change rate is caused by big fragments turning into tiny droplets or moving out of the selected region. The massive break-up shown in Figure 10 (b) fits the result of d=2.5 mm.

Similar results were found for higher injection pressures. Different break-up types were mostly determined by the distance of the laser focus to the axis of the nozzle. The main differences of the results at higher injection pressures from the one shown in Figure 11 were that, as the injection pressure increased, the peaks right after the laser pulse became smaller and the spray area change rate was more fluctuating. There were two main reasons for the difference. One was that there were more spontaneous break-ups due to higher injection pressure, so the proportion of the bubble collapse induced break-ups to the total break-up events was smaller. The other one was that the amount of laser light energy going into bubble formation was likely reduced due to a less smooth jet surface as the injection pressure became higher.

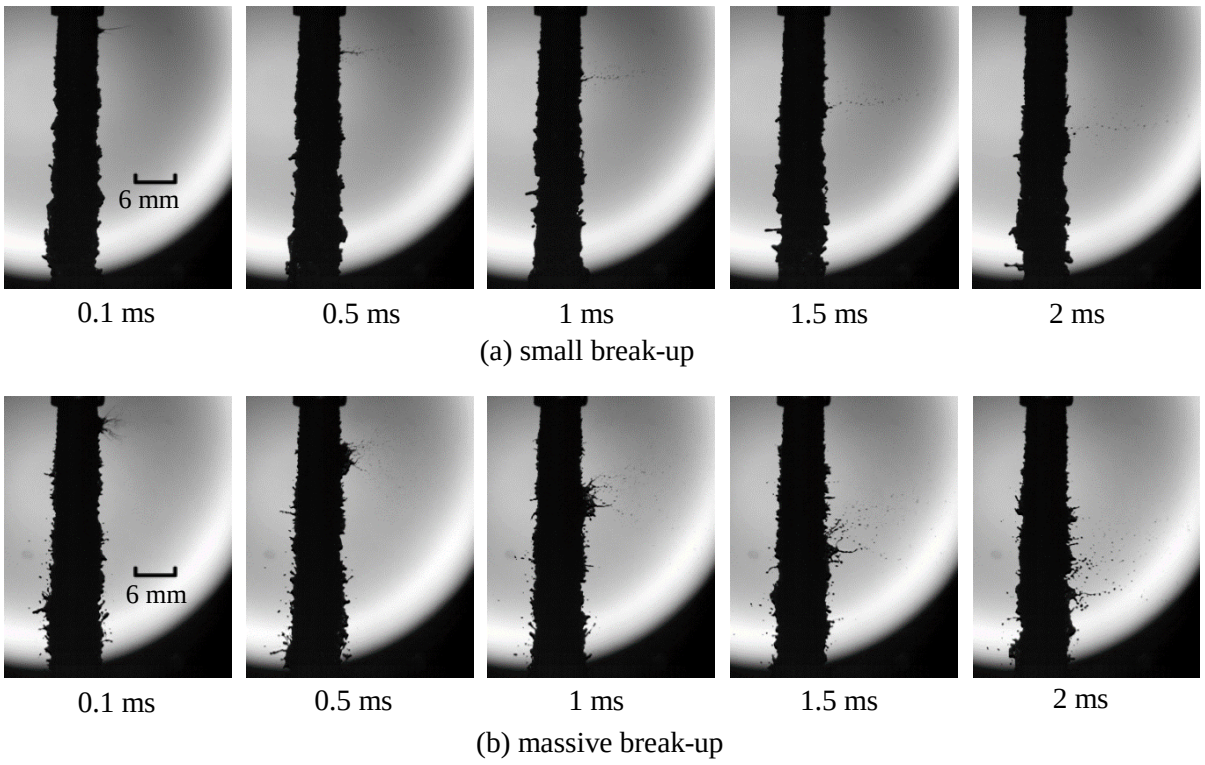

Figure 10 Small and massive break-ups at different conditions. (a) d=1.5 mm, P=1.6 bar. (b) d=2.5 mm, P=3.6 bar. The times indicated under each image is the time after the laser pulse.

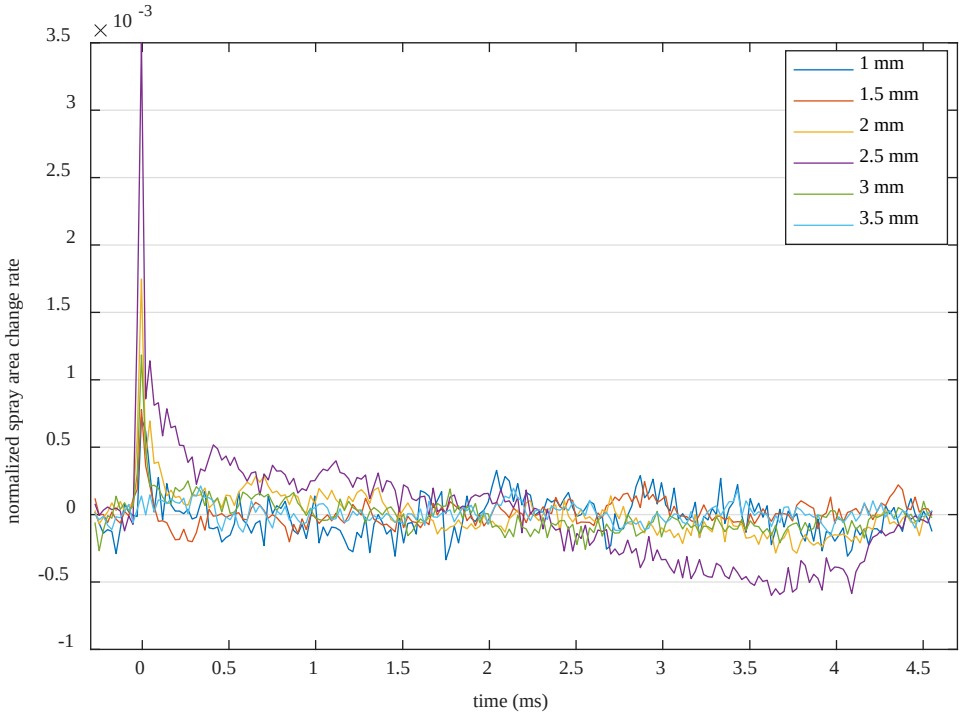

Figure 11 Normalized spray area change rate as a function of time after the laser pulse for various d when the injection pressure was 1.1 bar.

Cavitation bubbles outside the nozzle orifice were visualized in the study of Payri et. al. [35]. This investigation indicates the possibility that cavitation bubbles can pass through the orifice and collapse outside the nozzle. The in-nozzle cavitating flow and primary break-up region of

spray were studied with LES simulation by Örley et. al. [27] who showed the collapse events inside the jet caused an acceleration of liquid towards the liquid-gas interface and a small, high velocity liquid spike emerging from the jet surface. The current study confirmed the mechanism presented in these previous studies and showed that the position of the cavitation bubble is crucial for the break-ups. It's necessary to mention that the cavitation bubbles in the current study were introduced by laser and were much bigger than the ones in the other studies. However, when related to the study in chapter 3, similar assumption can be made that the bubble position together with the bubble size has big influence on the break-up events, which means that when the bubbles are smaller but closer to the jet surface, similar effects are expected to influence the break-ups.

More details of the study can be found in Paper II.

5 Conclusions

5.1 Free surface deformation induced by bubble collapse

The dynamics of laser-induced cavitation bubbles (growth, collapse, rebound) in different experimental geometries was investigated by Schlieren and shadow imaging. To avoid multiple bubbles, the laser beam was expanded before focused into the water to make a good focus. In a first set of experiments bubbles were introduced in water in a cuvette using different laser pulse energies. As the laser pulse energy goes higher, the maximum diameter the bubble is larger, and the period of the bubble growth and collapse is longer. This result is in agreement with previous studies [3,39,40].

Free surface deformation induced by cavitation bubble collapse near the surface was also studied. The dimensionless variable γ, which is the ratio of the distance of the initial bubble centroid to the free surface divided by the maximum bubble radius, was used to specify different experimental cases. The γ value was varied from 0.86 to 2.24 by adjusting the position of the laser beam focus. The main observations are summarized as following:

- For the cases of γ=0.86 and 0.94, both narrow spike and thick jets were observed at the free surface. The spike and thick jet started during the collapsing and rebounding phase of the bubble respectively. The spike jet developed faster than the thick jet, and the thick jet had a crown-shaped top.
- For the case of γ=1.10, the spike jet grew slower than the thick jet and merged together with the thick jet. When γ was 1.27, there was no spike jet but a small deformation formed during the four phases of bubble evolution and later merged with the thick jet. The velocity of the merged jet front was lower than the spike and thick jets and the thick/merged jets had a rounded top.
- For the cases of larger γ values from 1.52 to 2.24, there was no deformation at the free surface during the initial four phases of bubble evolution. The deformation appeared when the bubbles had moved far away from the free surface, and consisted of a dome-shaped protrusion widening and sinking back without liquid ejection. When the γ value was larger than 2.24, no obvious deformation at the free surface could be observed.

The current study performed a wider range of γ values which made it possible to cover the full evolution from narrow fast spikes to wider jets to reversing protrusions.

5.2 Bubble collapse induced liquid jet break-up

An experimental setup was established to introduce laser-induced cavitation bubbles into the primary break-up region of spray. Shadow images of the bubble collapse-induced break-up events were recorded by a high-speed video camera. Break-ups at different experimental conditions were analyzed, compared, and then categorized into two characteristic types, small and massive break-up. The projected spray area change rate was introduced and implemented to analyze the relationship between the experimental parameters and the types of jet break-up. The distance of the laser focus to the center axis of the nozzle was found to be the main factor that determined the type of break-up. As the flow velocity increased, i.e. higher Reynolds number, the spontaneous break-up events increased, and the relative strength of the bubble-

induced break-ups was reduced. The break-ups were very intense when the laser focus was located at 2.5 mm from the nozzle central axis, compared to a deeper or shallower focus. At low injection pressure conditions, i.e., the Reynolds number was roughly lower than $2 \cdot 10^5$, the structure of bubble collapse induced break-ups were much larger than the spontaneous ones. When the injection pressure went higher, i.e., the Reynolds number was roughly larger than $3 \cdot 10^5$, the difference between these two break-ups was smaller, especially further downstream of the sprays.

Both of the studies of bubble collapse induced free surface break-up and liquid jet break-up showed that the distance of the bubble to the liquid-gas interface had great influence on the surface deformation. So this parameter could be a key for further study of bubble collapse induced jet break-up.

6 Outlook

The current study has revealed the bubble-collapse induced free surface deformation under different γ values. It was done by adjusting the distance of the bubble to the free surface while the bubble size was almost constant. However, when the bubble size is different, the results may be different. Similar experiments with different sizes of bubbles were done in the studies by Patrascioiu et. al. [12] and Zhang et. al. [40]. Less violent thick jets, which had rounder jet front and lower relative height with respect to the bubble size, were observed in [12] when the bubble size was at the scale of 100 μm, but the γ value was similar. While in the study of [40], the thick jets were more violent when the bubbles were generated by a spark between electrodes and the size was at the scale of 20 to 30 mm. Therefore it would be interesting to do more experiments in which the γ value is constant and bubble size varies. One more reason that caused the difference between the results of current study and [12] might be the different liquid. In [12], a water and glycerol solution which had higher viscosity and lower surface tension was used. So experiments with different liquids would be valuable as well.

The deformations of the cavitation bubble and free surface were observed by experiments. However, the fluid dynamics of the surrounding fluid and the detailed structure of the deformation are still not clear enough. So relevant high-resolution simulations would be helpful to give more comprehensive description to the bubble and free surface interaction.

Although the turbulent jet experiments, which were presented in Paper II, were performed at conditions closer to those of diesel or gasoline spray in internal combustion engines, experimental data of liquid jets in conditions closer to laminar flow are more in need for developing SGS models. So the experiment in which the jet is smooth without any turbulence would be valuable for validation of simulation since the introduced bubble would be in a more well-defined environment, hence the shot-to-shot reproducibility will be higher at those conditions, and could be a link between the quiescent conditions in the cuvette and the highly turbulent conditions in the high-Re-number jet.

In the current study, the projected spray area change rate has been used to analyse the relationship between the laser focus position and the jet break-up. However, it does not present the spatial distribution of the break-ups and is impossible to distinguish the bubble collapse induced break-ups from the spontaneous ones when the injection pressure is high. Thus, it would be helpful to develop an image processing method to illustrate the spatial distribution of the break-up induced by bubble collapse in a statistical way.

References

[1] C. E. Brennen, *Cavitation and bubble dynamics* (Cambridge University Press, 2014).
[2] C. Ji, B. Li, J. Zou, and H. Yang, Experimental Thermal and Fluid Science **81**, 76 (2017).
[3] P. Koukouvinis, M. Gavaises, O. Supponen, and M. Farhat, Physics of Fluids **28**, 052103 (2016).
[4] N. Kyriazis, P. Koukouvinis, and M. Gavaises, Proceedings of the Royal Society A: Mathematical, Physical and Engineering Sciences **475**, 20180548 (2019).
[5] D. Obreschkow, P. Kobel, N. Dorsaz, A. de Bosset, C. Nicollier, and M. Farhat, Physical Review Letters **97**, 094502 (2006).
[6] E.-A. Brujan, K. Nahen, P. Schmidt, and A. Vogel, Journal of Fluid Mechanics **433**, 251 (2001).
[7] E.-A. Brujan, K. Nahen, P. Schmidt, and A. Vogel, Journal of Fluid Mechanics **433**, 283 (2001).
[8] I. Lentacker, I. De Cock, R. Deckers, S. C. De Smedt, and C. T. W. Moonen, Advanced Drug Delivery Reviews **72**, 49 (2014).
[9] G. L. Chahine, Journal of Fluids Engineering **99**, 709 (1977).
[10] J. R. Blake and D. C. Gibson, Journal of Fluid Mechanics **111**, 123 (1981).
[11] P. B. Robinson, J. R. Blake, T. Kodama, A. Shima, and Y. Tomita, Journal of Applied Physics **89**, 8225 (2001).
[12] A. Patrascioiu, J. M. Fernández-Pradas, J. L. Morenza, and P. Serra, Applied Surface Science **302**, 303 (2014).
[13] A. Patrascioiu, J. M. Fernández-Pradas, A. Palla-Papavlu, J. L. Morenza, and P. Serra, Microfluidics and Nanofluidics **16**, 55 (2014).
[14] O. Supponen, P. Kobel, D. Obreschkow, and M. Farhat, Physics of Fluids **27**, 091113 (2015).
[15] J. B. Keller and I. I. Kolodner, Journal of Applied Physics **27**, 1152 (1956).
[16] V. K. Kedrinskii, Acta Astronautica **3**, 623 (1976).
[17] W. F. Xie, T. G. Liu, and B. C. Khoo, Applied Numerical Mathematics **57**, 734 (2007).
[18] A. M. Zhang, X. L. Yao, and X. B. Yu, Journal of Sound and Vibration **311**, 1196 (2008).
[19] H. Kleine, S. Tepper, K. Takehara, T. G. Etoh, and K. Hiraki, (Springer Berlin Heidelberg, Berlin, Heidelberg, 2009), pp. 895.
[20] J. Li and J.-l. Rong, Ocean Engineering **38**, 1861 (2011).
[21] N. V. Petrov and A. A. Schmidt, Experimental Thermal and Fluid Science **60**, 367 (2015).
[22] J. Bohandy, B. F. Kim, and F. J. Adrian, Journal of Applied Physics **60**, 1538 (1986).
[23] F. J. Adrian, J. Bohandy, B. F. Kim, A. N. Jette, and P. Thompson, Journal of Vacuum Science & Technology B: Microelectronics Processing and Phenomena **5**, 1490 (1987).
[24] A. Piqué *et al.*, Journal of Materials Research **15**, 1872 (2000).
[25] C. B. Arnold, P. Serra, and A. Piqué, MRS Bulletin **32**, 23 (2007).
[26] M. Duocastella, A. Patrascioiu, J. M. Fernández-Pradas, J. L. Morenza, and P. Serra, Opt. Express **18**, 21815 (2010).
[27] F. Örley, T. Trummler, S. Hickel, M. S. Mihatsch, S. J. Schmidt, and N. A. Adams, Physics of Fluids **27**, 086101 (2015).
[28] W. H. Nurick, Journal of Fluids Engineering **98**, 681 (1976).
[29] C. Soteriou, R. Andrews, and M. Smith, (SAE International, 1995).
[30] T. Hayashi, M. Suzuki, and M. Ikemoto, in *12th Triennial International Conference on Liquid Atomization and Spray Systems, ICLASS*2012), pp. 2.
[31] J. Hult, P. Simmank, S. Matlok, S. Mayer, Z. Falgout, and M. Linne, Experiments in Fluids **57**, 49 (2016).
[32] A. Sou, S. Hosokawa, and A. Tomiyama, International Journal of Heat and Mass Transfer **50**, 3575 (2007).

[33] N. Mitroglou, M. Gavaises, J. M. Nouri, and C. Arcoumanis, in *Droplet Impact Phenomena and Spray Investigations Workshop 2011*, edited by G. E. Cossali, and S. Tonini (Dip. Ingegneria industriale. Università degli studi di Bergamo, Bergamo, Italy, 2011), pp. 33
[34] M. Linne, Progress in Energy and Combustion Science **39**, 403 (2013).
[35] R. Payri, F. J. Salvador, J. Gimeno, and J. de la Morena, International Journal of Heat and Fluid Flow **30**, 768 (2009).
[36] Holistic Approach of Spray Injection through a Generalized Multi-phase Framework (HAoS), http://haos-itn.eu/.
[37] E. Robert, J. Lettry, M. Farhat, P. A. Monkewitz, and F. Avellan, Physics of Fluids **19**, 067106 (2007).
[38] T. Ogasawara, S. Ito, and H. Takahira, in *Proceedings of the 10th International Symposium on Cavitation (CAV2018)*, edited by J. Katz (ASME, New York, NY, 2018).
[39] A. Vogel, W. Hentschel, J. Holzfuss, and W. Lauterborn, Ophthalmology **93**, 1259 (1986).
[40] S. Zhang, S. P. Wang, and A. M. Zhang, Physics of Fluids **28**, 032109 (2016).
[41] J. R. Blake, B. B. Taib, and G. Doherty, Journal of Fluid Mechanics **181**, 197 (1987).
[42] A. Pearson, E. Cox, J. R. Blake, and S. R. Otto, Engineering Analysis with Boundary Elements **28**, 295 (2004).
[43] R. Payri, J. M. García, F. J. Salvador, and J. Gimeno, Fuel **84**, 551 (2005).
[44] H. K. Suh and C. S. Lee, International Journal of Heat and Fluid Flow **29**, 1001 (2008).

Appended Publications Paper I-II